Electrochimica Acta 55 (2010) 2223–2231

Contents lists available at ScienceDirect

Electrochimica Acta

journal homepage: www.elsevier.com/locate/electacta

Electrodeposited Ni–B alloy coatings: Structure, corrosion resistance and mechanical properties

Yu.N. Bekish, S.K. Poznyak*, L.S. Tsybulskaya, T.V. Gaevskaya

Research Institute for Physical Chemical Problems, Belarusian State University, Leningradskaya Str. 14, 220050 Minsk, Belarus

ARTICLE INFO

Article history:
Received 27 June 2009
Received in revised form
18 November 2009
Accepted 21 November 2009
Available online 26 November 2009

Keywords:
Ni–B coating
Electrodeposition
Corrosion resistance
Microhardness
Wear resistance

ABSTRACT

Ni–B alloy coatings with different boron content ranging from 4 to approximately 28 at.% were prepared by electrodeposition in a nickel-plating bath containing sodium decahydroclovodecaborate as a boron source. The influence of the boron concentration in the coatings on their structure, morphology, electrochemical and corrosion behavior, physico-mechanical and electrical properties was investigated using X-ray diffractometry (XRD), scanning electron microscopy (SEM), potentiodynamic polarization, electrochemical impedance spectroscopy (EIS) and other methods. It was found that the electrodeposited Ni–B coatings with relatively low boron content (≤8 at.%) are nanocrystalline and comprise a solid solution of boron in f.c.c. Ni lattice having a mixed substituted-interstitial type. Further increase in the boron content (up to 10–15 at.%) leads to the appearance of heterogeneous amorphous-nanocrystalline structure, and the coatings with a high boron content (20 at.% and above) are X-ray amorphous. Polarization measurements in neutral NaCl solutions showed that the Ni–B coatings with relatively low boron content demonstrate a potential region of low anodic currents associated with the passive film formation at the alloy surface. The anodic current in this potential region increases significantly with increasing the boron content above 10 at.%, suggesting the non-protective nature of the anodic film formed on the amorphous Ni–B alloys. Immersion tests monitored by EIS measurements revealed a significantly better corrosion performance of the Ni–B coatings with low boron content (4 at.%) in comparison with that of the amorphous coatings. The microhardness and wear resistance of the Ni–B coatings essentially increases with increasing the boron content. Maximum microhardness and wear resistance were found for the coatings containing 8 at.% B.

1. Introduction

In the last two decades, considerable attention has been given to metal–metalloid alloys with nanocrystalline and amorphous structure which demonstrate a number of new properties in comparison with those of pure metals or metal alloys. Among these materials, Ni–B alloy coatings are promising due to their high hardness and superior mechanical wear resistance [1–8]. After heat treatment, the wear resistance of nickel–boron can equal or even exceed that of hard chromium coatings [9–11].

Although a variety of techniques, such as thermal boriding of the surface, melt quenching, sputtering in vacuum, are available for the preparation of the Ni–B coatings, electro- and electroless plating processes have received widespread acceptance due to their less complex processing sequence and cost-effectiveness. Electroless Ni–B coatings can be obtained from baths containing strong reducing agents such as sodium or potassium borohydride [1–3,8,10–16] and different amine boranes (dimethylamine borane [17,18], pyridine borane [19]). As a rule, electroless deposition is performed at high temperature (70–90 °C) and high pH values (13–14). Ni–B alloy coatings can be also deposited electrochemically from the baths containing sodium borohydride [20], dimethylamine borane [4,21,22], trimethylamine borane [5], carborane ion ($C_2B_9H_{12}^-$) [23] and sodium decahydroclovodecaborate [6]. It should be noted that the electrochemical method offers several advantages in comparison with the electroless one, such as high rate and low temperature of deposition, stability of electrolyte, uniform distribution of boron in the deposit, ease control of the plating process. However, the mechanism of deposition and properties of electroplated Ni–B coatings have been less studied in comparison with those of electroless coatings.

Along with enhanced microhardness, wear resistance and electrical characteristics, practical application of Ni–B coatings requires their high corrosion resistance depending on a number of factors such as chemical composition of the resultant coatings, their morphology and structure. It should be noted that the researches concerning the corrosion stability of electroless and electrodeposited Ni–B coatings are scanty [13,16,24,25]. Sankara Narayanan

* Corresponding author. Tel.: +375 17 2264696; fax: +375 17 2264696.
E-mail address: poznyak@ua.pt (S.K. Poznyak).

0013-4686/$ – see front matter © 2009 Elsevier Ltd. All rights reserved.
doi:10.1016/j.electacta.2009.11.069

and Seshadri [13] and Dadvand et al. [25] have pointed out that the corrosion resistance of amorphous electroless Ni–B coatings is less than that of electroless Ni–P ones. Anik et al. revealed that the corrosion resistance of electroless Ni–B films increased with increasing the boron content in the range from 4.5 to 8 wt.% [16]. In addition, the electroless Ni–B coatings were found to suffer a decrease in corrosion resistance with heat treatment [13,16,25]. To our knowledge, the effect of boron content and coating structure on the corrosion resistance of electroplated Ni–B films has not yet studied.

In our earlier work [6], we proposed the bath formulation for electrochemical deposition of Ni–B coatings using sodium decahydroclovodecaborate as a source of boron and studied the influence of the electrolyte composition and plating conditions on the composition, structure, microhardness and contact resistance of the deposited alloys. Unlike other boron-containing additives, the use of sodium decahydroclovodecaborate allows to deposit uncracked Ni–B alloy coatings with a boron concentration varied over a wide range from 1 to 30 at.% B.

The main objective of the present work was to elucidate how the corrosion stability and wear resistance of the electrodeposited Ni–B alloys depend on their structure and composition. Potentiodynamic polarization technique and electrochemical impedance spectroscopy were applied to investigate the corrosion properties of the alloys. Furthermore, new data on the morphology and structure of the Ni–B coatings deposited in decahydroclovodecaborate-containing electrolyte were obtained.

2. Experimental

The Ni and Ni–B coatings were electrodeposited on a copper substrate with an area of 3 cm^2 from electrolyte containing 240 g L^{-1} $NiSO_4 \cdot 7H_2O$, 36 g L^{-1} $NiCl_2 \cdot 6H_2O$, 31 g L^{-1} H_3BO_3, 57 g L^{-1} Na_2SO_4 and 0.1–20 g L^{-1} sodium decahydroclovodecaborate ($Na_2B_{10}H_{10}$). The current density, temperature and pH of the electrolyte were maintained at 0.02 A cm^{-2}, 30 °C, 4.5, respectively. Hot rolled nickel plate (99.7%) was used as an anode. Anode was placed parallel with cathode in the bath, and the anode-to-cathode area ratio was 2:1. Ni–B coatings with different boron content (hereafter referred to as Ni–B*X*, where *X* is the boron concentration in atomic percents) were produced by adjusting the $Na_2B_{10}H_{10}$ concentration in the bath. The film thickness was estimated by gravimetric analysis and averages 20 μm. The boron content in the Ni–B coatings was determined by potentiometric titration in the presence of mannitol [26]. The structure of the coatings was characterized by HZG–4M diffractometer (Germany) with a CoK_α radiation. The lattice parameter *a* was determined using diffraction peaks (1 1 1), (2 0 0), (2 2 0) and (3 1 1). The average grain size was estimated from the (1 1 1) peak broadening using the Scherrer equation [27]. The surface morphology of the deposits before and after corrosion tests was examined by scanning electron microscopy (LEO 1420 microscope).

The polarization measurements were performed using a Gamry potentiostat and a conventional three-electrode two-compartment Pyrex glass cell. A Pt foil and an Ag/AgCl/KCl (sat.) electrode (+0.199 V vs. the SHE) with a Luggin probe were used as the counter and reference electrodes, respectively. The working electrode with an exposed area of 1 cm^2 was used in these measurements. The sweep rate was 0.5 mV s^{-1}. All measurements were performed in non-deaerated 3.5% aqueous NaCl solution.

Electrochemical impedance spectroscopy (EIS) measurements were carried out at room temperature during immersion tests (3.5% NaCl solution) in a three-electrode cell consisting of a saturated calomel reference electrode, a platinum foil as the counter electrode and the working electrode with an exposed area of 3 cm^2. The cell was placed in a Faraday cage to avoid any interference with external electromagnetic fields. The EIS measurements were performed using a Gamry potentiostat with a PCI4 Controller in a frequency range from 5×10^4 to 3×10^{-3} Hz with a step of 7 points per decade. All the EIS spectra were recorded at open circuit potential with applied 10 mV sinusoidal perturbation. Before the spectra recording, the system was allowed to attain a stable open circuit potential. The impedance plots were fitted using different equivalent circuits by means of the Elchem Analyst software from Gamry.

Tribotechnical tests of the coatings were performed using an automated tribometer equipped by a special set-up for measurement of a coefficient of friction. Tribotechnical characteristics were measured under non-lubricated conditions at a specific load of 1 MPa. The film hardness (film thickness – 20 μm) was determined using a Viskers microhardness tester with a load of 1 N for 10 s of exposure, and the hardness values were averaged out of 10 determinations. Transient (contact) resistance of the films was assessed by the method based on measuring the resistance of a point contact of a reference electrode with the film at a load of 40 g.

3. Results and discussion

The introduction of sodium decahydroclovodecaborate in a nickel-plating electrolyte results in codeposition of boron with nickel. The boron content in the coating increases from 4 to approximately 28 at.% with the increase in the concentration of sodium decahydroclovodecaborate from 0.1 to 20 g L^{-1} (Fig. 1). The deposition rate is 24 ± 3 μm h^{-1} at $j_c = 0.02$ A cm^{-2}.

The current efficiency of the Ni–B plating increases from 95 to 100% and above with increasing the concentration of sodium decahydroclovodecaborate in electrolyte which is indicative of the presence of a concurrent reaction of Ni(II) reduction by sodium decahydroclovodecaborate at the cathode surface. When the $Na_2B_{10}H_{10}$ concentration exceeds 20 g L^{-1}, this undesirable chemical process begins to proceed with an appreciable rate in the solution bulk giving fine-dispersed Ni particles in electrolyte.

3.1. Structure of the coatings

Fig. 2 shows the results of the XRD study of Ni and Ni–B coatings. All coatings have face-centered cubic lattice of nickel. The main growth directions are [1 0 0] and [1 1 1]. The average grain size estimated for Ni coatings is 35–40 nm. Incorporation of 4 at.% B leads to the redistribution of the peak intensities corresponding to the (1 1 1) and (2 0 0) planes and to the decrease in average grain size up to 10–15 nm. The peak (1 1 1) becomes to be the most

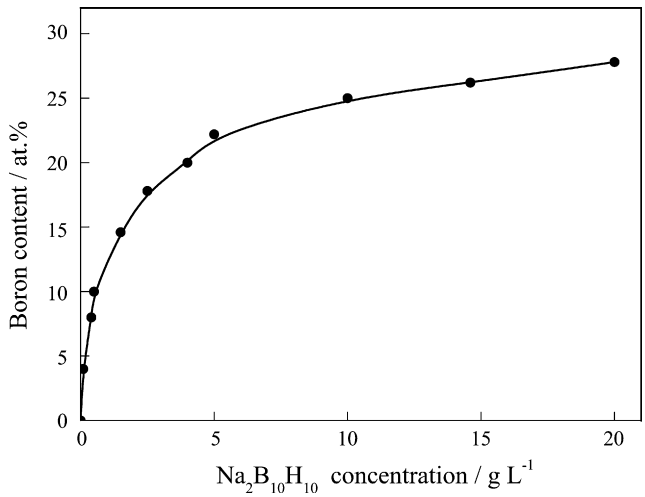

Fig. 1. Dependence of the boron content in Ni–B coatings on sodium decahydroclovodecaborate concentration in the electroplating bath.

intensive and the relative intensity of the peaks (2 2 0) and (3 1 1) increases slightly. With increasing the boron content up to 8 at.%, the intensity of peaks (2 0 0), (2 2 0) and (3 1 1) reduces. These peaks disappear at 10 at.% B and an amorphous phase arises (Fig. 2). The average grain size decreases up to 5–7 nm. The coatings with the B content more than 20 at.% are X-ray amorphous (Fig. 2).

When incorporating 4 at.% B in the coating, the f.c.c. lattice parameter a decreases from 3.524 to 3.508 Å. This decrease in the lattice spacing can be related to the replacement of nickel atoms having bigger atomic radius (r_{Ni} = 1.24 Å) by boron atoms with smaller atomic radius (r_{Ni} = 0.97 Å). The f.c.c. lattice parameter for the Ni–B alloy, calculated under assumption that the Ni atoms are replaced by B atoms, is significantly less ($\boldsymbol{a}_{\mathbf{calc}}$ = 3.493 Å for alloy with 4 at.% B) than the experimentally observed one. Since it is known that boron atoms due to their small size can occupy octahedral interstitial sites in the f.c.c. Ni lattice, it is possible to assume that nanocrystalline Ni–B coatings are a solid solution of boron in the f.c.c. Ni lattice having a mixed substituted-interstitial type. The formation of the substitutional solid solution can be indicative of the codeposition of boron in the elementary form. When increasing the boron content up to 8 at.% B, the lattice parameter is not appreciably changed. The estimation of the lattice parameter is difficult for the Ni–B coatings with the boron content more than 8 at.%, because the peak (1 1 1) is strongly broadened and the other peaks disappear.

3.2. Morphology of the coatings

Fig. 3 shows the surface morphology of the boron-free Ni coatings and Ni–B alloy ones with different boron content. The rough and dull surface of the Ni coating (Fig. 3) consisting of pyramidal crystallites turns into more smooth and bright one as boron atoms are incorporated into the film and their content increases. At 4 at.% B, the surface becomes nodular and spherical particles differ widely in size (Fig. 3). The nodular structure with "orange peel" shape becomes more clearly defined and the size of spherical particles becomes more uniform in going to the X-ray amorphous coatings.

3.3. Polarization measurements

Fig. 4 presents typical polarization curves for the Ni and Ni–B coatings with different B content in 3.5% NaCl solution. Anodic and cathodic branches of the polarization curves were recorded separately at freshly prepared electrodes at a low scanning rate of 0.5 mV s^{-1}. As can be seen from Fig. 4 increasing the B content does not influence noticeably the rate of the oxygen electroreduction occurring in the potential range from −0.3 to −0.8 V, and at more negative potentials only a slight increase in the overpotential for hydrogen evolution is observed.

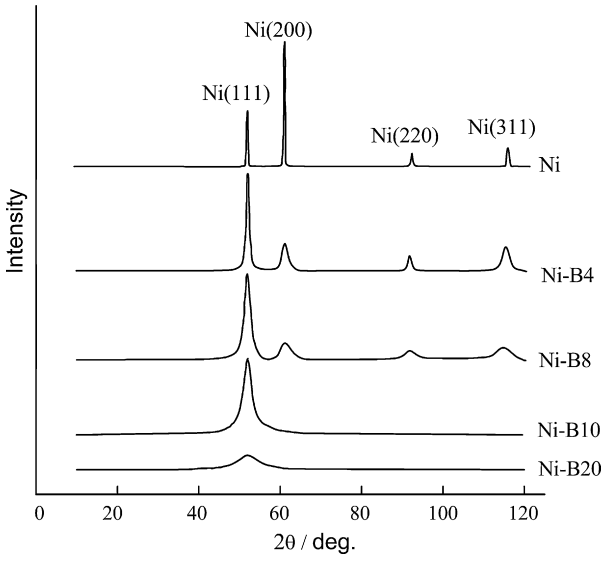

Fig. 2. X-ray diffraction patterns of nickel and Ni–B coatings.

Unlike the cathodic reactions, the boron doping exerts a stronger effect on the anodic processes of film oxidation. The electrodeposited boron-free Ni coatings and Ni–B coatings with a relatively low B content (≤10 at.%) are characterized by the presence of a region of low anodic currents in the potential range from corrosion potential to about 0 V (Fig. 4). After stopping the potential sweep in this region, the current drops rapidly up to very low values (less than 1 μA cm^{-2}), indicating that the passive oxide film formation occurs in this potential region (Fig. 5, insert). At more positive potentials, the breakdown of the passive film takes place due to the interaction of the aggressive chloride ions with the passivated surface [28], and the anodic current begins to grow exponentially. The boron doping leads to the shift of the corrosion potential to the negative direction. The anodic polarization curves are changed most significantly in going from nanocrystalline to amorphous Ni–B coatings when increasing the B content from 10 to 20 at.% and higher. An appreciable growth of the anodic current is observed for the amorphous coatings in the potential range from −0.3 to 0 V, and a current step appears at potentials from −0.16 to −0.18 V (Fig. 4). Fig. 5 shows the current vs. time dependence recorded at a fixed potential of −0.16 V chosen in the region of the current step. After stopping the potential sweep the current initially continues to grow with time and then begins to drop gradually until reaching quasi-stationary values (70–80 μA cm^{-2}) which are essentially higher than those observed for the nanocrystalline Ni–B coatings. SEM inspection of the surface morphology after 7 h of holding the Ni–B20 electrode at a potential of −0.16 V showed that a distinctive etching of the surface with the formation of fine (hundreds of nanometers) and larger (about 1 μm) pits takes place, i.e. under these conditions the anodic pitting dissolution of the coating occurs (Fig. 6).

Thus, the results of the polarization measurements testify that a high content of boron in the Ni–B coatings can lead to appreciable deterioration of the corrosion resistance of these materials in neutral chloride solutions.

3.4. Immersion corrosion tests and EIS measurements

Prolonged immersion tests monitored by impedance measurements were performed to gain a better understanding of the corrosion behavior of Ni–B coatings. Impedance spectra of the Ni and Ni–B samples were recorded at different times after immersion of the samples in non-deaerated 3.5% NaCl solution. Typical impedance spectra after 24 and 168 h of immersion are shown in Fig. 7. The Nyquist impedance diagrams have the form of slightly depressed semicircle, and in most cases, only one time constant can be observed on the Bode plots in the frequency range studied. In the case of amorphous Ni–B20 and Ni–B26 coatings, Warburg diffusion behavior was observed in the low frequency region, indicating that the corrosion mechanism is controlled not only by a charge transfer step but also by a diffusion process. A simple equivalent circuit composed of the solution resistance, R_{sol}, in series with a parallel connection of the capacitance of double layer, Q_{dl}, and the charge transfer resistance, R_{ct}, was used for interpretation of the impedance spectra revealing only one time constant for nanocrystalline Ni and Ni–B coatings (Fig. 8a). After 168 h of immersion, an additional time constant appears on the impedance spectrum of the Ni–B10 coatings in low frequency region (0.1–1 Hz) (Fig. 9). This time constant can be associated with the corrosion processes in pits appeared, as will be shown below, on the sample surface

during the immersion test. In this case, we used a more complicated equivalent circuit for fitting of impedance spectra with two additional elements, Q_{cor} and R_{cor}, for describing the corrosion process in the pits (Fig. 8b). For amorphous Ni–B coatings, a Warburg element describing the diffusion process was added to the equivalent circuit (Fig. 8c). In the equivalent circuits used, the double layer capacitance C_{dl} and the capacitance C_{cor} are represented by a constant phase element (Q), which accounts for the deviation from

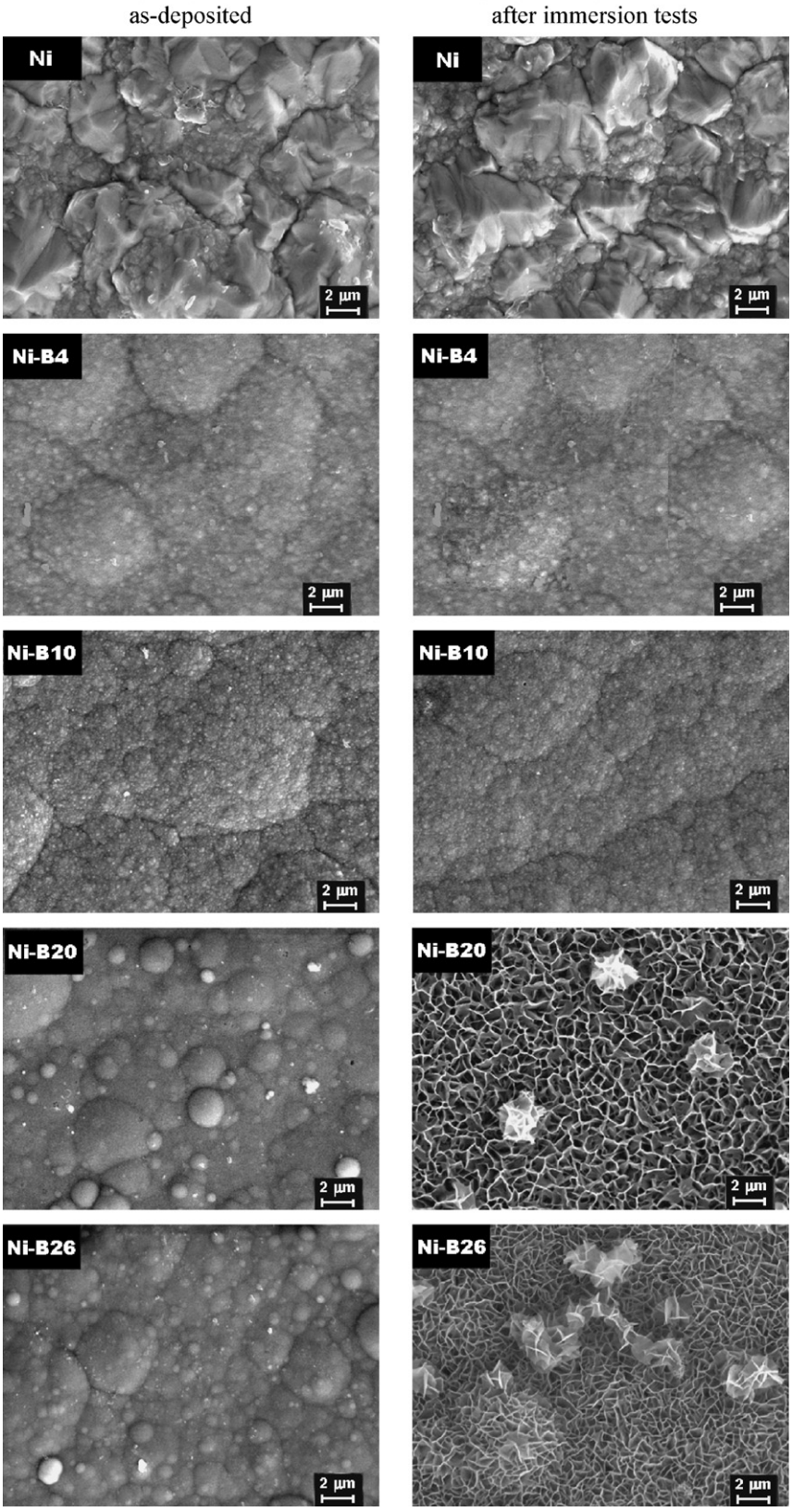

Fig. 3. SEM micrographs of the surface of as-deposited Ni and Ni–B coatings and the coatings after immersion tests in 3.5% NaCl solution for 3 weeks.

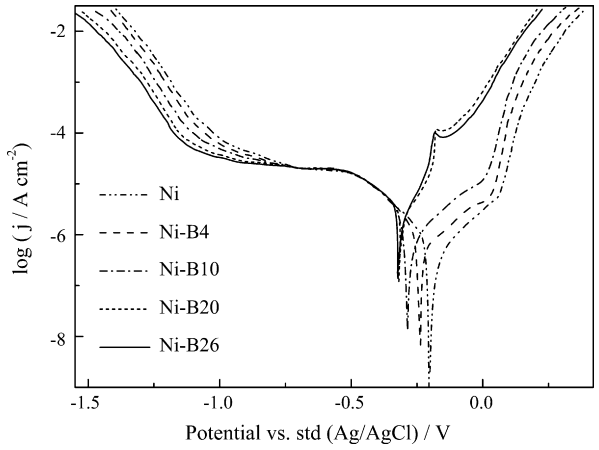

Fig. 4. Polarization curves of Ni and Ni–B coatings in 3.5% aqueous NaCl solution. Scanning rate was 0.5 mV s^{-1}.

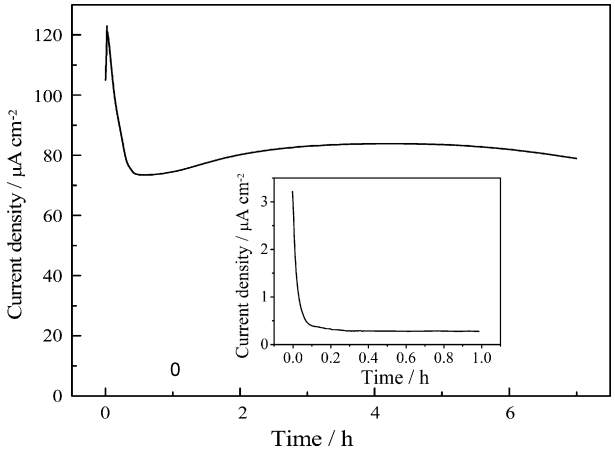

Fig. 5. The current vs. time curves recorded during anodic oxidation of the Ni–B20 and Ni–B4 (insert) coatings in 3.5% NaCl solution at a fixed potential of −0.16 and −0.06 V, correspondingly. Initially the potential was swept from the corrosion potential to −0.16 V for Ni–B20 and −0.06 V for Ni–B4 at a scanning rate of 0.5 mV s^{-1}.

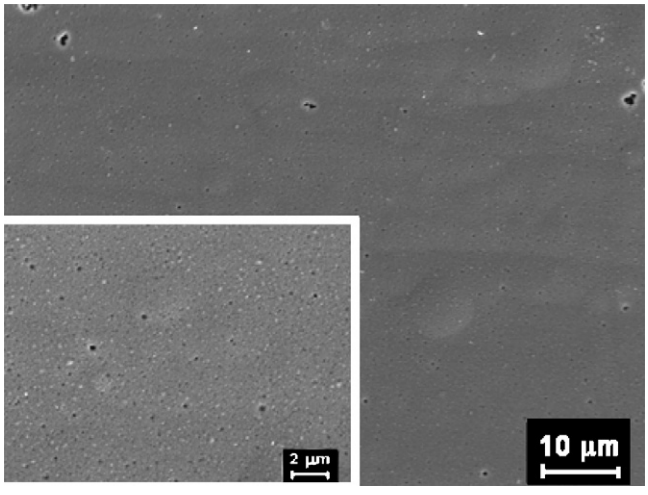

Fig. 6. SEM micrographs (at two different magnifications) of the surface of Ni–B20 electrode after keeping in 3.5% NaCl solution for 7 h at a fixed potential of −0.16 V.

the ideal dielectric behavior of the non-ideal capacitor. The capacitance values for the capacitive elements in the equivalent circuits were calculated using the following equation:

$$C = Q(\omega_{max})^{n-1}, \quad (1)$$

where Q is the constant phase element, ω_{max} the frequency at which the imaginary impedance reaches a maximum for the corresponding time constant [29].

The calculated equivalent circuit parameters at different times of sample immersion in chloride solution are presented in Figs. 10 and 11. It should be noted that the behavior of nanocrystalline boron-free Ni coatings and Ni–B ones with a relatively low B content (≤10 at.%) is different from that of the amorphous Ni–B coatings with a high B content. At the beginning of immersion, the nanocryslalline coatings demonstrate the R_{ct} values in the range from 50 to 100 kOhm cm^2 (Fig. 10a, inset). The charge transfer resistance increases rapidly (especially in the first hour) with immersion time, reaches maximum values and then begins to decrease. For the Ni–B4 coatings, maximum values of R_{ct} range from 7100 to 7500 kOhm cm^2 as compared with those (5800 to 6000 kOhm cm^2) for boron-free Ni coatings (Fig. 10a). When increasing the B content up to 10 at.%, the $R_{ct\ max}$ decreases several times. The double layer capacitance of Ni and Ni–B4 coatings remains in a rather narrow interval (21–26 μF cm^{-2}) and is close to the values usually attributed to the double layer capacitance on metals (Fig. 11a). For the Ni–B10 coatings, the C_{dl} initially varies insignificantly (21–23 μF cm^{-2}). Then after 170 h of immersion, the capacitance starts to grow reaching limiting values of 31–33 μF cm^{-2} after 300 h of immersion (Fig. 11a).

The initial rapid rise in the charge transfer resistance for nanocrystalline Ni and Ni–B coatings can be related to the formation and growth of a thin passive film on the metal surface. SEM studies showed that the surface morphology of the nanocrystalline Ni and Ni–B coatings is not appreciably changed after the immersion test, indicating that the formed passive film is very thin (Fig. 3a–c). Although these coatings have a dense micro- or nanocrystalline structure, corrosion-active species from electrolyte can penetrate gradually to the copper substrate along the grain boundaries or finest pores or pinholes and initiate the corrosion process, resulting in the formation of corrosion pits on the surface. As a consequence, the charge transfer resistance of the electrode system starts to drop after several days of immersion. Inspection of the sample surface after the immersion tests actually revealed several corrosion pits on the Ni and Ni–B10 coatings.

Other behavior is observed in the case of amorphous Ni–B coatings with a high B content. On immersing into NaCl solution, these coatings demonstrate significantly lower R_{ct} values (15–25 kOhm cm^2) in comparison with those for the nanocrystalline ones (Fig. 10b). Moreover, the charge transfer resistance even decreases slightly during the first hour of immersion, indicating that the active corrosion process occurs on the metal surface (Fig. 10b, inset). Then the R_{ct} begins to grow, reaches a maximum, decreases and finally again grows after approximately 170 h of immersion. It should be noted that the maximum values of R_{ct} for amorphous Ni–B coatings are significantly lower (fall in the range 100–150 kOhm cm^2) than those for nanocrystalline Ni and Ni–B coatings. Some rise in the R_{ct} after an hour may be associated with the formation of a film of corrosion products on the surface which is not so protective as in the case of nanocrystalline Ni and Ni–B coatings. Further decrease in the R_{ct} seems to be related to the appearance of minute local pits on the corroded surface. Accumulation of the corrosion products impedes further action of the electrolyte, leading to the Warburg diffusion behavior and to gradual decrease in the corrosion rate. Actually Ni–B20 and Ni–B26 samples after corrosion tests demonstrate the appearance of colored film on the surface. SEM examination of the corroded

Ni–B20 and Ni–B26 coatings revealed the presence of a film of corrosion products with a specific nanostructure (Fig. 3). The enhanced C_{dl} values observed for these samples after prolonged immersion are probably related to the high porosity of the corroded surface (Fig. 11b).

Thus, the results of EIS studies are in good agreement with the data of polarization measurements and testify that the corrosion resistance of nanocrystalline Ni–B coatings is essentially higher than that of amorphous Ni–B coatings with a high B content. This enhanced corrosion resistance is due to the formation of a compact protective oxide film on the metal surface. The Ni–B coatings with a low boron content (4 at.%) demonstrate the maximum corrosion resistance in chloride solutions which may be caused by a sharp decrease in the grain size for these coatings in comparison with boron-free Ni ones. This assumption is based on the results of Wang et al. who revealed that the corrosion resistance of the electrodeposited Ni coatings increased significantly as the grain size decreased from microcrystalline to nanocrystalline [30]. They explained this effect by the more rapid formation of a compact passive film on nanocrystalline Ni owing to a higher density of nucleation sites (grain boundaries and dislocations inside grains) for the passive film.

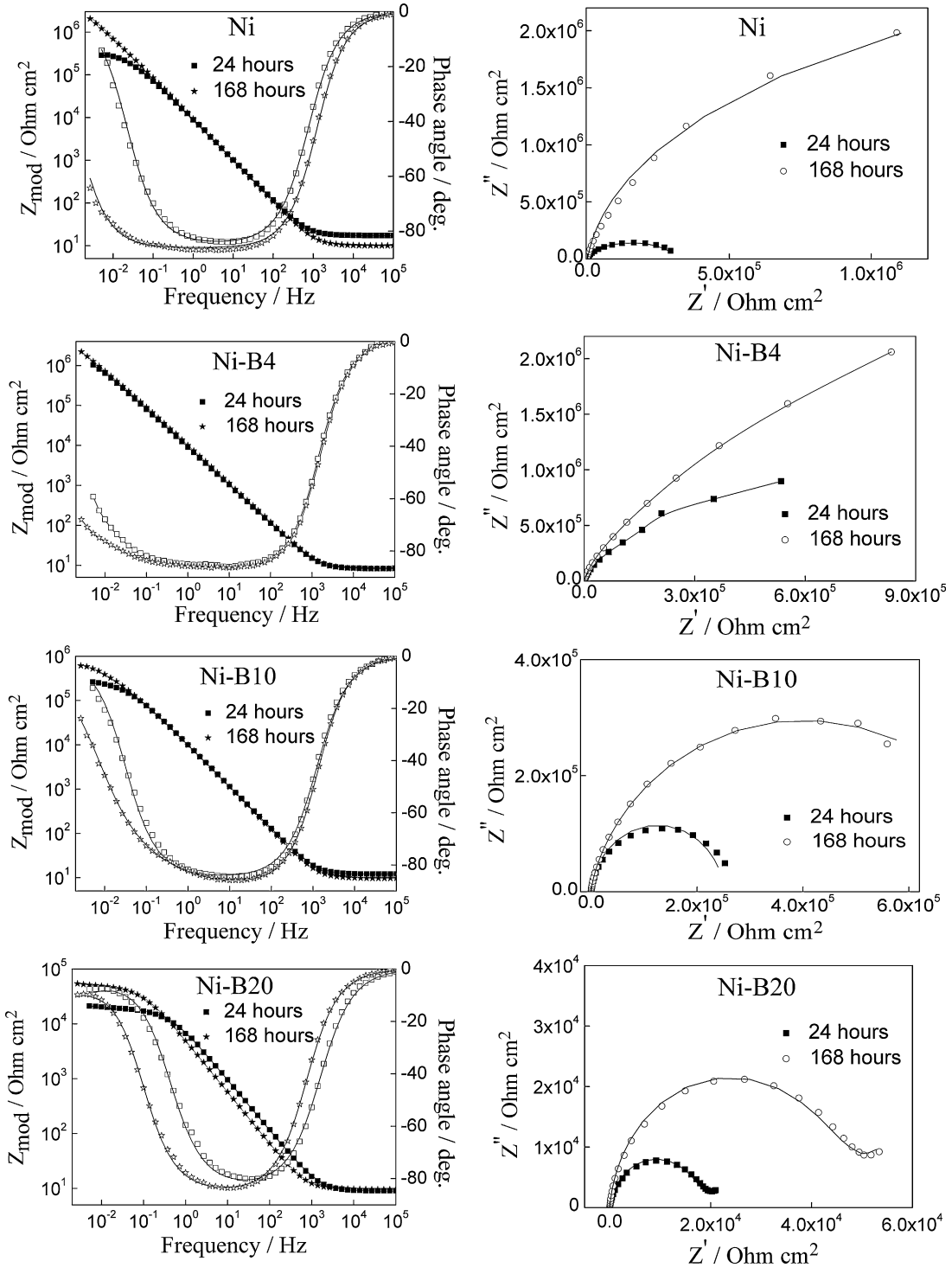

Fig. 7. Bode and Nyquist plots of the Ni and Ni–B coatings after 24 and 168 h of immersion in 3.5% NaCl solution.

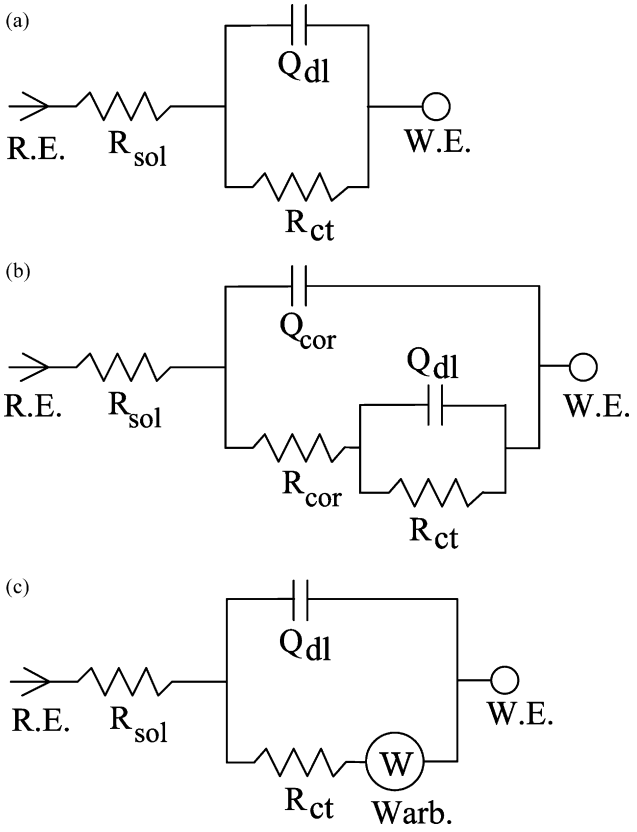

Fig. 8. Equivalent electrical circuit models used to analyze the EIS data for Ni and Ni–B coatings.

As the boron content increases up to 10 at.% in the Ni–B coatings, an amorphous phase appears in them and their corrosion resistance decreases. Probably in such heterogeneous coatings the corrosion processes can be accelerated due to the formation of local minute galvanic couples between crystalline and amorphous phases. In addition, the increase in the boron content can lead to degradation of protective properties of the forming passive film due to the increase in its defectiveness and loosening. This effect is most pronounced in the case of amorphous Ni–B coatings. They have no region of film passivity on the anodic polarization curves, and during prolonged immersion tests, a relatively thick film of corrosion products is formed on the coating surface, which does not fulfill the function of a protective film to prevent the development of corrosion processes.

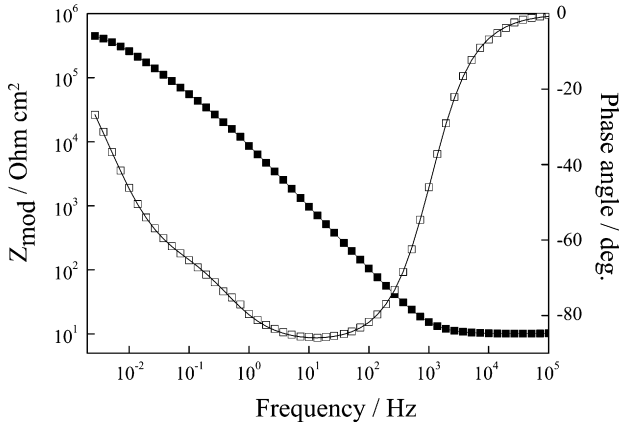

Fig. 9. Bode plot of the Ni–B10 coating after 168 h of immersion in 3.5% NaCl solution.

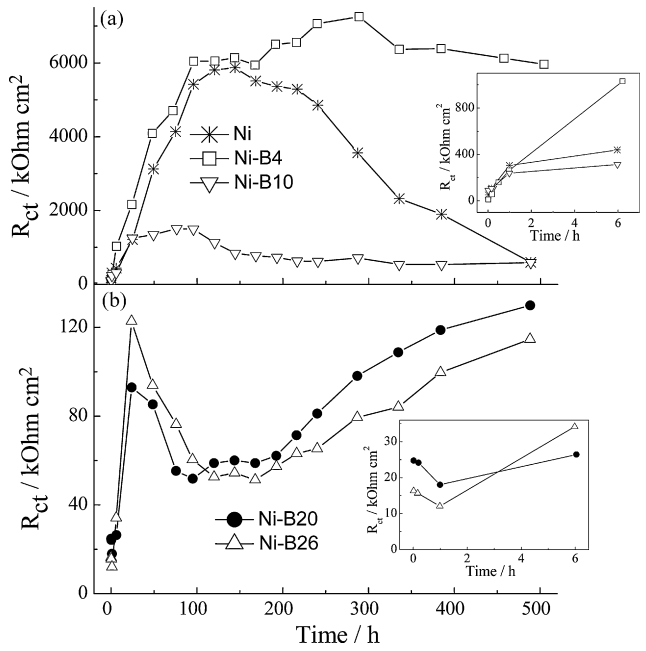

Fig. 10. Time evolution of the charge transfer resistance of (a) Ni and nanocrystalline Ni–B coatings and (b) amorphous Ni–B coatings during the immersion in 3.5% NaCl solution. Insets show time evolution of the charge transfer resistance at the beginning of immersion.

3.5. Mechanical and electrical properties of the coatings

Data on the influence of composition of Ni–B coatings on their mechanical and electrical properties are presented in Fig. 12 and Table 1. As can be seen from Fig. 12, the rapid transition to a linear stage of steady-state wear is characteristic of the boron-free nickel

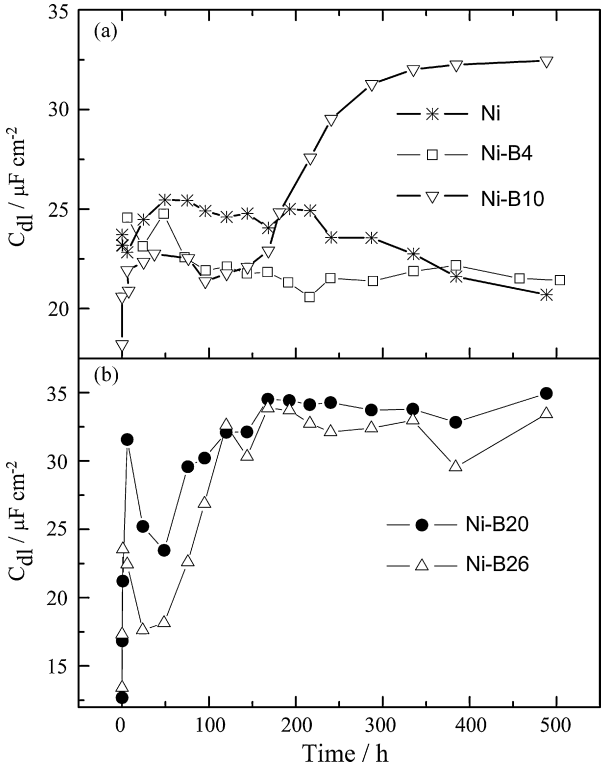

Fig. 11. Time evolution of the double layer capacitance of (a) Ni and nanocrystalline Ni–B coatings and (b) amorphous Ni–B coatings during the immersion in 3.5% NaCl solution.

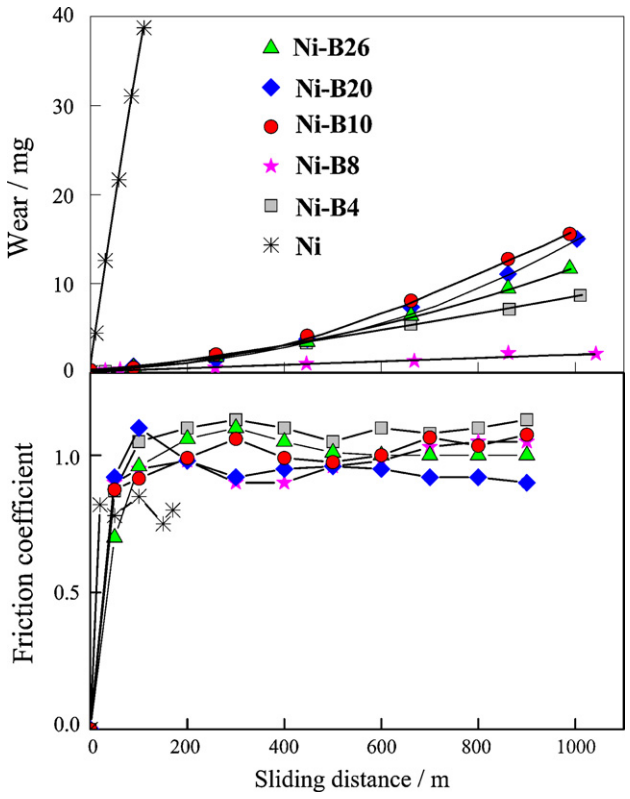

Fig. 12. The wear and friction coefficient vs. sliding distance for Ni and Ni–B coatings.

coating. The Ni coating wears out completely after a sliding distance of 100 m. The wear rate for the Ni coating is 39.1×10^{-2} mg m^{-1} (Table 1), the friction coefficient ranges from 0.7 to 0.85 (Fig. 12) and the microhardness is 2400 MPa (Table 1). Incorporation of boron into the Ni coating leads to a significant increase in its microhardness, wear resistance and friction coefficient (Fig. 12 and Table 1). The lowest wear rate (0.2×10^{-2} mg m^{-1}) and the highest microhardness (8500 MPa) are observed for the nanocrystalline Ni–B8 coating. The appearance of amorphous phase in the Ni–B coatings at a boron content of 10 at.% leads to the decrease in microhardness and wear resistance. For the amorphous Ni–B coatings, the microhardness and wear resistance again increase in comparison with Ni–B10 coatings. Thus, the appreciable deterioration of the mechanical properties is observed for the Ni–B coatings including both nanocrystalline and amorphous phases. The following consideration could explain this effect. It is known that along with heating, the plastic deformation can initiate the crystallization of amorphous materials. This effect was named as mechanical crystallization [31]. The formation of crystalline domains in amorphous coatings on friction can result in appearance of considerable tensile stresses at the interface due to a substantial difference in specific atomic volumes of amorphous and crystalline phases. Since it is known that interfacial deformations can significantly decrease the breaking strength of materials during frictional interaction or cyclic loading [32], the formation of crystalline domains in amorphous coatings under friction can result in the deterioration of wear-resisting properties of such materials. At the same time, gain in stability of amorphous phases should be accompanied by a rise in the wear resistance of the coatings. Thus, the materials with a metastable amorphous-crystalline structure possessing an enhanced tendency to the mechanical crystallization, such as Ni–B10 coatings, should demonstrate low tribotechnical characteristics.

Table 1
Microhardness (H_μ), wear rate (I_q), coefficient of friction (f) and contact electrical resistance (R) of the boron-free nickel and Ni–B alloy coatings with different boron content.

Boron content (at.%)	H_μ (MPa)	I_q (mg m^{-1})	f (a.u.)	R (mOhm)
–	2400	0.391	0.7–0.85	2.8
4	7600	0.008	0.9–1.1	3.4
8	8500	0.002	0.9–1.0	4.3
10	7300	0.014	1.0–1.1	5.8
20	7800	0.011	0.9–1.0	12.8
25	8000	0.009	1.0–1.1	16.8

The Ni–B coatings with nanocrystalline structure have a rather low contact resistance (3–4.5 mOhm) only slightly higher than that of boron-free Ni (Table 1). At the same time, the amorphous Ni–B coatings demonstrate sufficiently high values of the contact resistance (13–17 mOhm).

4. Conclusions

The following main conclusions can be drawn from this study:

(1) At the boron content ≤8 at.%, electrodeposited Ni–B coatings have nanocrystalline structure and are comprised of a solid solution of boron in f.c.c. Ni lattice having a mixed substitutional-interstitial type. The Ni–B coatings with a medium boron content (approximately 10 at.%) demonstrate amorphous-nanocrystalline structure, and the coatings with a high boron content (20 at.% and above) are X-ray amorphous.
(2) The corrosion resistance of the nanocrystalline Ni–B coatings is essentially higher than that of the amorphous ones. The Ni–B coatings with a relatively low boron content (4 at.%) demonstrate a maximal corrosion resistance which even exceeds the corrosion resistance of boron-free Ni coatings.
(3) The increase of the boron content in the homogeneous nanocrystalline Ni–B coatings leads to a significant increase in their microhardness and wear resistance. For the coatings with heterogeneous amorphous-nanocrystalline structure, these mechanical characteristics are somewhat deteriorated. The further amorphization of the Ni–B coatings at a high B content again results in an improvement of the mechanical properties.

Thus, the electrodeposited nanocrystalline Ni–B coatings with relatively low boron content demonstrate rather high corrosion resistance, essentially enhanced microhardness and wear resistance, rather low contact resistance and are promising for different applications.

Acknowledgement

This work was partially supported by the Belarusian Republican Foundation for Fundamental Research (Project no. X09 GKNT-006).

References

[1] F. Delaunois, J.P. Petitjean, P. Lienard, M. Jacob-Duliere, Surf. Coat. Technol. 124 (2000) 201.
[2] F. Delaunois, P. Lienard, Surf. Coat. Technol. 160 (2002) 239.
[3] K. Krishnaveni, T.S.N. Sankara Narayanan, S.K. Seshadri, Surf. Coat. Technol. 190 (2005) 115.
[4] K. Krishnaveni, T.S.N. Sankara Narayanan, S.K. Seshadri, Mater. Chem. Phys. 99 (2006) 300.
[5] K.H. Lee, D. Chang, S.C. Kwon, Electrochim. Acta 50 (2005) 4538.
[6] T.V. Gaevskaya, I.G. Novotortseva, L.S. Tsybulskaya, Met. Finish. 94 (1996) 100.
[7] P. Vassiliou, J. Novakovic, Rev. de Metalurgia (Madrid) (Special issue) (2005) 232.
[8] Z. Shi, D. Wang, Z. Ding, Appl. Surf. Sci. 221 (2004) 62.
[9] R.N. Duncan, T.L. Arney, Plat. Surf. Finish. 71 (1984) 49.
[10] B. Oraon, G. Majumdar, B. Ghosh, Mater. Des. 29 (2008) 1412.
[11] C.T. Dervos, J. Novakovic, P. Vassiliou, Mater. Lett. 58 (2004) 619.
[12] H. Li, H. Li, W. Dai, M. Qiao, Appl. Catal. A: Gen. 238 (2003) 119.

[13] T.S.N. Sankara Narayanan, S.K. Seshadri, J. Alloys Compd. 365 (2004) 197.
[14] Q. Rao, G. Bi, Q. Lu, H. Wang, X. Fan, Appl. Surf. Sci. 240 (2005) 28.
[15] I. Baskaran, R. Sakthi Kumar, T.S.N. Sankara Narayanan, A. Stephen, Surf. Coat. Technol. 200 (2006) 6888.
[16] M. Anik, E. Korpe, E. Sen, Surf. Coat. Technol. 202 (2008) 1718.
[17] W. Evans, M. Shlesinger, J. Electrochem. Soc. 141 (1994) 78.
[18] A. Contreras, C. Leon, O. Jimenez, E. Sosa, R. Perez, Appl. Surf. Sci. 253 (2006) 592.
[19] M. Matsuoka, T. Hayashi, Plat. Surf. Finish. 68 (1981) 66.
[20] C.R. Pichard, Z. Bouhala, A.J. Nosser, A. Rashid, J. Mater. Sci. 20 (1985) 3305.
[21] O. Motonobu, T. Takeshi, J. Surf. Finish. Soc. Jpn. 41 (1990) 388.
[22] K. Krishnaveni, T.S.N. Sankara Narayanan, S.K. Seshadri, Trans. Indian Inst. Met. 56 (2003) 341.
[23] G.A. Sadakov, A.Y. Ezikyan, F.I. Kukoz, Sov. Electrochem. 16 (1980) 1507.
[24] T.S.N. Sankara Narayanan, K. Krishnaveni, S.K. Seshadri, Mater. Chem. Phys. 82 (2003) 771.
[25] N. Dadvand, W.F. Caley, G.J. Kipouros, Can. Metall. Quart. 43 (2004) 229.
[26] Y.I. Valsyunene, P.K. Norkus, Trudy Akademii Nauk Litovskoj SSR. Ser. B 1 (1972) 93.
[27] V.I. Iveronova, G.P. Revkevich, The Theory of X-ray Scattering, MGU, Moscow, 1972.
[28] B. MacDougall, J. Electrochem. Soc. 126 (1979) 919.
[29] C.S. Hsu, F. Mansfeld, Corrosion 57 (2001) 747.
[30] L. Wang, J. Zhang, Y. Gao, Q. Xue, L. Hua, T. Xu, Scripta Mater. 55 (2006) 657.
[31] M. Trudeau, R. Shulz, D. Dussault, Phys. Rev. Lett. 64 (1990) 99.
[32] V.A. Kukareko, Trenie i Iznos (Friction and Wear) 24 (2003) 192.